Controlled synthesis of octahedral jarosite

Zhongchun Li[1,2] ✉, *Xia Xu*[2], *Zhixian Wang*[2], *Hongying Lv*[2], *Xianghong He*[2], *Liangbiao Wang*[2]

[1]*Jiangsu Key Laboratory of Precious Metals Chemistry and Engineering, Changzhou, 213001, People's Republic of China*
[2]*School of Chemistry and Environmental Engineering, Jiangsu University of Technology, Changzhou, 213001, People's Republic of China*
✉ *E-mail: czlizc@126.com*

Published in Micro & Nano Letters; Received on 10th July 2018; Revised on 16th September 2018; Accepted on 1st October 2018

Octahedral jarosite was successfully prepared without extra template using a novel hydrothermal route based on the redox reaction between $KMnO_4$ and $(NH4)_2Fe(SO_4)_2{\cdot}6H_2O$. The mass ratio of $(NH_4)_2Fe(SO_4)_2{\cdot}6H_2O/KMnO_4$, reaction time, and reaction temperature play key roles in forming octahedral crystals. The chemical composition and microstructure of as-prepared octahedral jarosite were characterised by X-ray diffraction, scanning electron microscopy, energy dispersive spectrum, high-resolution transmission electron microscopy, and selective area electron diffraction. The formation mechanism of octahedral jarosite was discussed preliminarily.

1. Introduction: Morphology-controlled synthesis is an important research branch because small changes in the morphology of particle can result in spectacular influences on the physical and chemical properties [1–3]. In recent years, great efforts were made to controlled-synthesis of micro/nanocrystals with different morphologies [4–6]. However, preparation of inorganic crystals with complex architectures is highly desirable. Jarosite ($KFe_3(SO_4)_2(OH)_6$) is a yellow, hydrous sulphate of K^+ and Fe^{3+} found in many geological conditions, and it is of great interest in the field of geology, environment, and metallurgy [7, 8]. Jarosite forms commonly in the acid conditions by the oxidation of sulphides [9]. Various routes have been explored to the preparation of jarosite. For example, Tuovinen and co-authors [10] reported the synthesis of jarosite using bacteria to oxidation of ferrous sulphate. McCubbin's group applied hydrothermal route to the preparation of jarosite [11]. Despite the progress, there was little literature to report the controlled-synthesis of jarosite crystals with perfect morphology. A perfect morphology is the one that contains no linear, or planar imperfections. The polyhedral jarosite crystals should own regular architecture with well-defined edges and sharp corners. For octahedral jarosite crystals, the specific facets will be exposed, which is beneficial to further applications such as catalysis and environment, electrochemistry. Thus, it is desirable to the controllable synthesis of jarosite with perfect morphology. In this case, a novel hydrothermal route was developed to the growth of jarosite with uniform octahedral or truncated octahedral morphology, which is based on the redox reaction between $KMnO_4$ and $(NH_4)_2Fe(SO_4)_2{\cdot}6H_2O$ without extra surfactant or template. The mass ratio between $KMnO_4$ and $(NH_4)_2Fe(SO_4)_2{\cdot}6H_2O$, reaction time, and reaction temperature play vital roles in forming octahedral jarosite.

2. Experimental

2.1. Chemicals and reagents: Ammonium iron (II) sulphate hexahydrate $(NH_4)_2Fe(SO_4)_2{\cdot}6H_2O$, potassium permanganate ($KMnO_4$), and ethanol (EtOH) were analytical pure and used without further purification.

2.2. Synthesis of octahedral jarosite: Octahedral jarosite was synthesised by a novel hydrothermal route as follows. $KMnO_4$ (0.20 g) was firstly dissolved into 15 ml H_2O, followed by adding $(NH_4)_2Fe(SO_4)_2{\cdot}6H_2O$ (2.0 g) under stirring vigorously. Then the solution was poured into a 25 ml of Teflon-lining, which was sealed in steel autoclave. After hydrothermal treatment for 16 h at 140°C in an oven, the autoclave was cooled down naturally. The precipitate was collected by centrifugation, followed by washing with H_2O and EtOH at least three times. To obtain uniform octahedrons, the rotate speed of centrifuge should be strictly controlled. Finally, the yellow sample was dried at 60°C under vacuum.

2.3. Characterisation: The morphology and element composition were analysed by scanning electron microscopy (SEM, HITACHI-3400s) and energy dispersive spectrum (EDS). The microstructure was observed by high-resolution transmission electron microscopy (HRTEM, FEI Tecnai G2 F30). The crystal structure was tested by X-ray diffraction (XRD).

3. Results and discussion

3.1. Morphologies and microstructures of jarosite: XRD pattern of as-prepared octahedral jarosite is described in Fig. 1. Each peak in Fig. 1 can be readily indexed to a hexagonal phase of jarosite with lattice constants $a=b=7.29$ Å, $c=17.16$ Å, $\alpha=\beta=90°$, $\gamma=120°$, which is compatible with the literature value (JCPDS Card No. 22-0827) [12], and the sharpness of the peaks implies the prepared jarosite is well crystallised. No obvious impurity peaks were found, suggesting that pure octahedral jarosite was synthesised in this case. A typical SEM image of octahedral jarosite is displayed in Fig. 2*a*. It can be clearly observed that the as-prepared jarosite crystals own perfect octahedral architecture with well-defined edges and sharp corners. As depicted in Fig. 2*a*, the edge lengths of octahedrons are in the range of 3–5 μm. Energy dispersive spectrum was applied to detect the element composition. The signals of K, Fe, O and S elements were found on the EDS spectrum (Fig. 2*b*), revealing the existence of K, Fe, O and S in octahedral jarosite. And the atomic ratio between K and Fe is about 1:4.5.

To further understand the microstructure of octahedral jarosite, structural analyses were carried out by HRTEM and selective area electron diffraction (SAED). Fig. 2*c* presents a representative TEM image of octahedral jarosite. Perfect octahedral architectures were shown in Fig. 2*c*. The inset in Fig. 2*c* shows the SAED pattern of octahedral jarosite, which indicates that the as-prepared octahedral jarosite is a single crystal in nature. The continuous lattice fringes of as-prepared octahedral jarosite can be seen in Fig. 2*d*. The space between neighbouring lattice planes is 0.37 nm, which is in line with the (110) planes of the hexagonal phase of jarosite.

doi: 10.1049/mnl.2018.5376

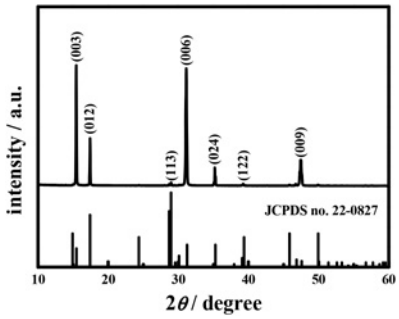

Fig. 1 *XRD pattern of as-prepared octahedral jarosite*

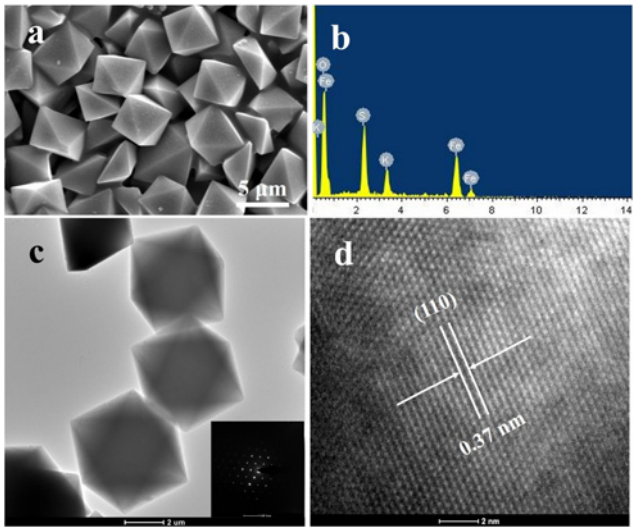

Fig. 2 *Characterisation of octahedral jarosite*
a SEM image of octahedral jarosite
b EDS pattern
c TEM image (the inset is the corresponding SAED pattern)
d HRTEM image

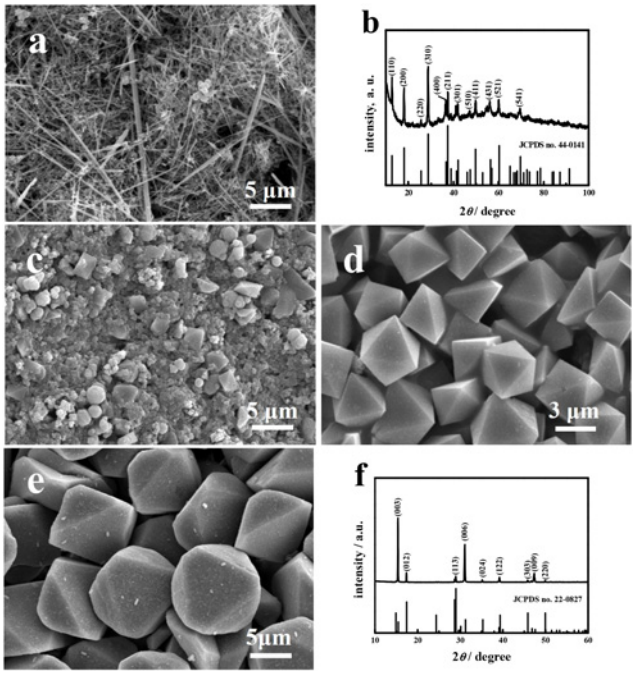

Fig. 3 *SEM images of samples synthesised at different mass ratios of* $(NH_4)_2Fe(SO_4)_2{\cdot}6H_2O/KMnO_4$
a 1.0
b 1.0 and XRD pattern
c 5.0
d 7.5
e 20
f 20 and XRD pattern

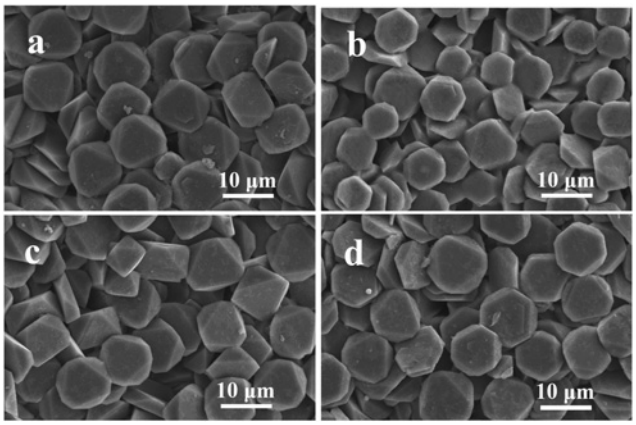

Fig. 4 *SEM images of jarosites synthesised at different reaction time at the* $(NH_4)_2Fe(SO_4)_2{\cdot}6H_2O/KMnO_4$ *mass ratio of 10. Reaction time (h)*
a 2
b 4
c 6
d 8

3.2. Influence of experimental conditions on the formation of octahedral jarosite: Comparative experiments were carried out at the different mass ratio between $(NH_4)_2Fe(SO_4)_2{\cdot}6H_2O$ and $KMnO_4$. Figs. 3*a* and *c*–*e* display the SEM images of samples synthesised at various mass ratios of $(NH_4)_2Fe(SO_4)_2{\cdot}6H_2O/KMnO_4$. MnO_2 nanorods could be obtained when the mass ratio of $(NH_4)_2Fe(SO_4)_2{\cdot}6H_2O/KMnO_4$ is 1.0 (Fig. 3*a*). Fig. 3*b* presents the corresponding XRD pattern of MnO_2 nanorods, which can be indexed to tetragonal α-MnO_2 (JCPDS Card No. 44-0141) [13–15]. α-MnO_2 was formed from the redox reaction between Fe^{2+} ions and MnO_4^- ions, which can be described as the following equation:

$$MnO_4^- + 3Fe^{2+} + 4H^+ \rightarrow MnO_2 + 3Fe^{3+} + 2H_2O \qquad (1)$$

When the mass ratio of $(NH_4)_2Fe(SO_4)_2{\cdot}6H_2O/KMnO_4$ was increased to 5.0, the sample was made up of the mixture of polyhedrons and small particles, as shown in Fig. 3*c*. The octahedral crystals with well-defined edges could be achieved when the mass ratio of $(NH_4)_2Fe(SO_4)_2{\cdot}6H_2O/KMnO_4$ was raised to 7.5 or 10.0 (Figs. 3*d* and 2*a*). When the mass ratio of $(NH_4)_2Fe(SO_4)_2{\cdot}6H_2O/KMnO_4$ was increased to 20.0, the truncated corners could be obtained (Fig. 3*e*). Fig. 3*f* shows the XRD pattern of the truncated octahedron, which can be attributed to the hexagonal phase of jarosite (JCPDS Card No. 22-0827). With the mass ratio of $(NH_4)_2Fe(SO_4)_2{\cdot}H_2O/KMnO_4$ increasing, the concentrations of K^+, SO_4^{2-}, and Fe^{3+} ions were increased in the mixed system, which interacted each other to produce jarosite. From the above results, it can be concluded that the mass ratio between $(NH_4)_2Fe(SO_4)_2{\cdot}6H_2O$ and $KMnO_4$ was a crucial prerequisite for the formation of octahedral jarosite crystals.

Fig. 4 presents the SEM images of samples prepared at various reaction time. When the reaction time is short (Figs. 4*a* and *b*), truncated octahedrons are dominant product. As time goes on, a small number of octahedral crystals were found in the samples, as shown in Figs. 4*c* and *d*. Octahedral crystals with well-defined

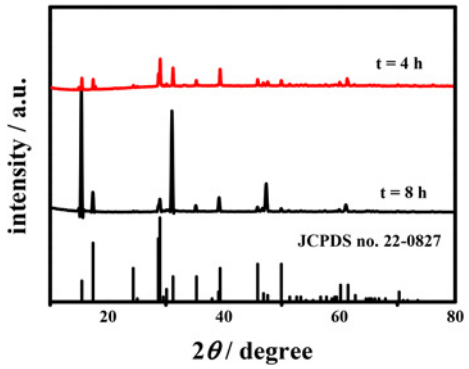

Fig. 5 *XRD patterns of samples synthesised at different reaction time*

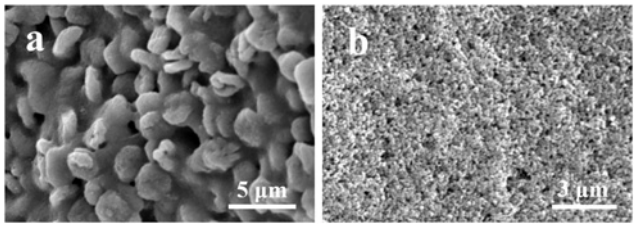

Fig. 6 *SEM images of samples synthesised at the different reaction temperature. Reaction temperature (°C)*
a 120
b 180

edges were prepared when the hydrothermal time was extended to 16 h (Fig. 2*a*). The XRD patterns of samples prepared at 4 and 8 h were also examined, and the corresponding results presented in Fig. 5 indicate that all samples can be indexed to the hexagonal phase of jarosite (JCPDS Card No. 22-0827). From the relative intensity of peaks, it can be concluded that the crystallinity increases with the reaction time. Thus, the reaction time is an important influence factor on the morphologies.

Fig. 6 shows the SEM images of the samples prepared at different temperature with an $(NH_4)_2Fe(SO_4)_2{\cdot}6H_2O/KMnO_4$ mass ratio of 10. When the experiment was carried out at 120°C (Fig. 6*a*), biscuits-like structures were prepared. However, nanoparticles were achieved when the reaction temperature was enhanced to 180°C (Fig. 6*b*). Therefore, the reaction temperature is also a crucial factor in the sample's morphologies.

3.3. Growth mechanism of octahedral jarosite: The inorganic crystal growth habit depends on their relative order of surface energies when they are prepared under hydrothermal condition [16, 17]. The crystal will grow in the direction, which is perpendicular to that with the highest surface energy. This leads to the fade away of planes with higher energies. By contrast, the lattice planes with lower energy enhance in surface area. As described in previous literature, the morphology evolution of crystals depends on the growth rate ratio (R) between (100) and (111) direction [6, 18]. The polyhedron was obtained when $R = 0.87$. When R is in the range of 0.87–1.73, the truncated octahedron was formed. An ideal octahedron was achieved when R is 1.73. In this case, $KFe_3(SO_4)_2(OH)_2$ crystal nucleus were firstly produced from the redox reaction between $KMnO_4$ and $(NH_4)_2Fe(SO_4)_2{\cdot}6H_2O$ in aqueous solution under the hydrothermal condition, which would act as crystal seeds to the growth of octahedrons or truncated octahedrons. When the hydrothermal reaction time is short, R should be in the range of 0.87–1.73, resulting in forming truncated octahedrons. As time goes on, R was increased to 1.73. At this stage, octahedral crystals were obtained.

4. Conclusion: In summary, a novel hydrothermal route is developed to the synthesis of octahedral jarosite based on the redox reaction between $KMnO_4$ and $(NH_4)_2Fe(SO_4)_2{\cdot}6H_2O$. The reaction time, reaction temperature, and mass ratio of $(NH_4)_2Fe(SO_4)_2{\cdot}6H_2O/KMnO_4$ have significant impacts on forming octahedral jarosite. The formation mechanism of octahedral jarosite was discussed preliminarily.

5. Acknowledgments: This work was supported by the National Natural Science Foundation of China (grant nos. 21701061 and 51872129), and Natural Science Foundation of Jiangsu Province (grant no. BK20160292).

6 References

[1] Xiong X., Waller G., Ding D., *ET AL.*: 'Controlled synthesis of $NiCo_2S_4$ nanostructured arrays on carbon fiber paper for high-performance pseudocapacitors', *Nano Energy*, 2015, **16**, pp. 71–80
[2] Tomboc G.M., Jadhav H.S., Kim H.: 'PVP assisted morphology-controlled synthesis of hierarchical mesoporous $ZnCo_2O_4$ nanoparticles for high-performance pseudocapacitor', *Chem. Eng. J.*, 2017, **308**, pp. 202–213
[3] Zhang L., Zhao Y., Lin Z., *ET AL.*: 'Kinetically controlled synthesis of large-scale morphology-tailored silver nanostructures at low temperature', *Nanoscale*, 2015, **7**, (32), pp. 13420–13426
[4] Lv X., Zhang H., Wang F., *ET AL.*: 'Controllable synthesis of MnO_2 nanostructures anchored on graphite foam with different morphologies for a high-performance asymmetric supercapacitor', *CrystEngComm*, 2018, **20**, (12), pp. 1690–1697
[5] Jiang P., Liu Q., Ge C., *ET AL.*: 'Cop nanostructures with different morphologies: synthesis, characterization and a study of their electrocatalytic performance toward the hydrogen evolution reaction', *J. Mater. Chem. A*, 2014, **2**, (35), pp. 14634–14640
[6] Xia Y., Xia X., Peng H.-C.: 'Shape-controlled synthesis of colloidal metal nanocrystals: thermodynamic versus kinetic products', *J. Am. Chem. Soc.*, 2015, **137**, (25), pp. 7947–7966
[7] Liu J.-S., Li B.-M., Zhong D.-Y., *ET AL.*: 'Preparation of jarosite by acidithiobacillus ferrooxidans oxidation', *J. Cent. South Univ. Tehcnol.*, 2007, **14**, (5), pp. 623–628
[8] Pappu A., Saxena M., Asolekar S.R.: 'Jarosite characteristics and its utilisation potentials', *Sci. Total. Environ.*, 2006, **359**, (1), pp. 232–243
[9] Baron D., Palmer C.D.: 'Solubility of jarosite at 4–35°C', *Geochim. Cosmochim. Acta.*, 1996, **60**, (2), pp. 185–195
[10] Grishin S.I., Bigham J.M., Tuovinen O.H.: 'Characterization of jarosite formed upon bacterial oxidation of ferrous sulfate in a packed-bed reactor', *Appl. Environ. Microb.*, 1988, **54**, (12), pp. 3101–3106
[11] McCubbin F.M., Tosca N.J., Smirnov A., *ET AL.*: 'Hydrothermal jarosite and hematite in a pyroxene-hosted melt inclusion in martian meteorite miller range (MIL) 03346: implications for magmatic-hydrothermal fluids on Mars', *Geochim. Cosmochim. Acta*, 2009, **73**, (16), pp. 4907–4917
[12] Amils R., De la Fuente V., Rodríguez N., *ET AL.*: 'Composition, speciation and distribution of iron minerals in *Imperata cylindrica*', *Plant Physiol. Biochem.*, 2007, **45**, (5), pp. 335–340
[13] Lu M., Lu Y., Qiu K., *ET AL.*: 'One-pot synthesized ultrathin MnO_2 nanorods as advanced electrodes for high-performance supercapacitors', *Mater. Lett.*, 2016, **166**, pp. 255–258
[14] Zhao T., Duan F., Jiang X., *ET AL.*: 'Hydrothermal synthesis of three structured MnO_2 nanomaterials and their performance for catalytic oxidation of resorcinol and formaldehyde', *Chem. Lett.*, 2016, **45**, (4), pp. 457–459
[15] Wang Y., Sun H., Ang H.M., *ET AL.*: '3D-hierarchically structured MnO_2 for catalytic oxidation of phenol solutions by activation of peroxymonosulfate: structure dependence and mechanism', *Appl. Catal. B, Environ*, 2015, **164**, pp. 159–167
[16] Li Z., Gu A., Zhou Q.: 'Growth of spindle-shaped silver nanoparticles in SDS solutions', *Cryst. Res. Technol.*, 2009, **44**, (8), pp. 841–844
[17] Li Z., Gu A.: 'Growth of spindle-shaped gold nanoparticles in cetyltrimethylammonium bromide solutions', *Micro Nano Lett.*, 2009, **4**, (3), pp. 142–147
[18] K. S.T., L. R.A.: 'Nonspherical noble metal nanoparticles: colloid-chemical synthesis and morphology control', *Adv. Mater.*, 2010, **22**, (16), pp. 1781–1804

doi: 10.1049/mnl.2018.5376